A hybrid density functional study of lithium in ZnO: Stability, ionization levels, and diffusion

A. Carvalho,[1] A. Alkauskas,[2] Alfredo Pasquarello,[3,4] A. K. Tagantsev,[1] and N. Setter[1]
[1]*Ceramics Laboratory, École Polytechnique Fédérale de Lausanne (EPFL), CH-1015 Lausanne, Switzerland*
[2]*Electron Spectrometry and Microscopy Laboratory, Institute of Condensed Matter Physics, École Polytechnique Fédérale de Lausanne (EPFL), CH-1015 Lausanne, Switzerland*
[3]*Institute of Theoretical Physics, École Polytechnique Fédérale de Lausanne (EPFL), CH-1015 Lausanne, Switzerland*
[4]*Institut Romand de Recherche Numérique en Physique des Matériaux (IRRMA), CH-1015 Lausanne, Switzerland*
(Received 7 July 2009; revised manuscript received 27 September 2009; published 12 November 2009)

The properties of interstitial and substitutional Li in wurtzite ZnO are modeled using hybrid density functional calculations. We investigate the impact of the band-gap error on the formation energies of the two defects and their dependence on the Fermi level. It is found that within a local-density approximation, the acceptor level of Li_{Zn} is very close to the valence-band top but as the band gap is opened, the acceptor state becomes more localized and the respective level is shifted upward. Taking polaronic effects into account, we place the ionization level of Li_{Zn} between $E_v+0.60$ eV and $E_v+1.1$ eV. This deeper level explains the difficulty in realizing *p*-type ZnO using Li as monodopant. Further, the mobility of the defects was investigated. While interstitial Li is mobile at low temperatures, independent of the stoichiometry, the diffusion of Li_{Zn} depends on the concentrations of intrinsic defects. Our calculations show that in O-rich material, where the defect is more stable, the dominant diffusion process corresponds to a dissociative mechanism requiring a substantial activation energy.

DOI: 10.1103/PhysRevB.80.195205 PACS number(s): 61.72.uj, 66.30.Lw, 61.72.Bb

I. INTRODUCTION

Zinc oxide (ZnO) is a multifunctional material combining a variety of exceptional piezoelectric, semiconducting, optical, and optoelectronic properties. Its numerous applications range from the traditional uses as piezoelectric transducer or transparent conducting electrodes to novel applications such as UV light-emitting diodes, transparent field-effect transistors, and nanostructure devices.[1] In Li-doped materials, there have been reports of an unusual electric polarization hysteresis loop and a temperature anomaly of the dielectric permittivity resembling ferroelectricity, which after being understood and controlled may inspire a whole new range of interesting applications.[2]

Obviously, the success of these developments requires the improvement of growth technologies for the fabrication of high-quality single crystals and epitaxial layers and processing techniques adequate to control the electrical and optical properties of the material. This relies on the understanding of the role of dopants and other impurities, as well as native defects which, despite major progress in the last few years, is still incomplete.

Perhaps the most striking limitation is the difficulty in realizing high-conductivity *p*-type ZnO. Since ZnO is often grown in Zn-rich conditions, it has generally been assumed in the past that O vacancies (V_O) or Zn interstitials (Zn_i) are responsible for the *n*-type conductivity of as-grown material and for the compensation of acceptor-type dopants.[1] The oxygen vacancy is a double donor and local density functional studies have consistently indicated that this defect possesses one of the lowest formation energies among donor-type defects.[3–6] Nevertheless, controversy has recently arisen when efforts to apply different gap correction schemes led to conflicting results for the formation energies and the positioning of the 0/++ level.[6–11]

Another difficulty resides in the choice of the doping element. Candidates include group-V elements substituting for O and group-III elements substituting for Zn, despite the large size mismatches in the latter case. Group I species such as Li and Na at the cation site have been predicted to be among the shallowest acceptors,[12] and recently, there have been a few reports of successful growth of Li-doped *p*-type thin films,[13,14] reviving the interest on the use of this element as monodopant. Notwithstanding, in general, Li doping is rather inefficient. One of the reasons is that coexisting with the substitutional form (Li_{Zn}), which is an acceptor, there is also an interstitial form (Li_i), a shallow donor. In principle, this problem can be overcome by controlling the substitutional rate and the resulting degree of self-compensation. However, it has recently been suggested that Li_{Zn} is not a shallow acceptor center as has been assumed,[15] and therefore it is unable to produce high-conductivity *p*-type material even in ideal conditions.

Experimental evidence of a shallow acceptor level has been forwarded by Hall-effect measurements and photoluminescence, cathodoluminescence, and photoconductivity studies which yield an acceptor level 110–300 meV above the valence band.[14,16–18] On the other hand, other experimental groups support the view that the same Li defect introduces a deep rather than a shallow level. Schiermer reported on the properties of an unusual excited center observable by electron paramagnetic resonance (EPR) spectroscopy under ultraviolet light excitation at 77 K and consisting of a hole trapped at an oxygen atom very close to the ionized Li impurity.[19,20] A characteristic feature of this paramagnetic center is a significant relaxation of the Li-O bond. This metastable defect state may persist up to 100–150 K when electrons released by the deep donors return Li_{Zn} to the Li_{Zn}^{-} ground state.[21] Later, the ionization energy associated with this transition, giving rise to radiative recombination, was

measured to be at least 500 meV.[15] This lead Meyer *et al.*[15,22] to argue that Li introduces a deep rather than a shallow acceptor, responsible for a broad luminescence band in the yellow spectral range (~2.1 eV). Later work observed the appearance of a Li-related shallow acceptor (~300 meV) upon annealing samples containing the deep acceptor in a hydrogen atmosphere, and offered an alternative explanation to the bound excitons at ~3.36 eV generally related to a shallow Li acceptor.[15,22,23] A paramagnetic Na_{Zn}^{0} center also exists and has given rise to a similar discussion.[15,24]

The properties of Li_i and to what extent it competes with Li_{Zn} are also not yet clear. Early Hall-effect measurements suggested that it is a hydrogenlike center with an ionization energy of about 5 meV,[25] however theory indicates that it ionizes spontaneously.[26] Due to its mobility,[21,27] the interstitial species have remained elusive, and it was not until recently that interstitial Li donors, confined to ZnO nanoparticles, were detected by electron-nuclear double-resonance (ENDOR) experiments.[28] The shallow character of the center is apparent through the dependence of the *g* factor on the size of the nanoparticles, and numerous ENDOR lines arising from the interaction with about 20 ^{67}Zn nuclei were observed.

Li defects in ZnO have been object of a few theoretical studies[12,26,29–31] but so far these have not been able to clarify the two issues fundamental for *p*-type doping: the region of stability of the substitutional form, and the position of its acceptor level. Initially, a very shallow acceptor state for Li_{Zn} was suggested by theoretical studies predicting an ionization energy of about 0.09–0.2 eV.[12,26,29] However, those calculations were performed using local density functional theory and suffer the consequences of its well-known underestimation of the band gap. This problem is particularly severe in ZnO—typically resulting in the band gap being underestimated to $E_g \sim 0.8$ eV whereas experimentally ZnO is known to have a band gap of ~3.4 eV at the Γ point. The band-gap underestimation causes difficulties to the interpretation of calculated defect formation energies and ionization levels. Electronic-structure calculations based on a hybrid functional,[30] found no localized one-electron state in the band gap, corroborating, to a certain point, the results of the local density functional calculations but information on transition levels is still lacking.

The challenge of modeling Li_{Zn} is not limited to the solution of the band-gap problem. The localized hole trapped by the Li acceptor is an example of a small bound polaron center. Bound polarons associated with aliovalent impurities are common in oxide crystals. Centers with similar properties include alkali metals in ZnO, BnO, and MgO and alkaline-earth oxides, and aluminum in silica (for reviews, see Refs. 32 and 33). The Al center in silica has been object of numerous theoretical studies addressing the problem of charge localization. It is known that the commonly used semilocal density functional theory approaches, as well as some hybrid density functional (HDF) schemes, fail to describe the structural relaxation around the Al impurity.[34,35] This failure is due to incomplete self-interaction cancellation, and the problem can be solved by treating the exchange interaction at the Hartree-Fock level. Similarly, semilocal density functional theory predicts a delocalized state for the hole trapped at Li (Refs. 12, 26, and 29) whereas EPR spectroscopy shows a strong localization at the closest axial O site.[19] Further, recent calculations using an on-site occupation-dependent potential have shown that the correct description of the defect-hole system can be obtained if the energies of the unoccupied hole states are correctly placed relative to the spectrum of occupied states.[31]

In this paper, we report on a density functional study of the properties of Li both in the substitutional and in the interstitial form. We employ both semilocal and hybrid density functionals for the exchange and correlation energy. The latter improves the description of the band edges and band-gap states, allowing us to explore the properties of the two fundamental Li defects for the full range of accessible Fermi energies. In addition, the hybrid functional improves the description of the exchange interaction and is able to provide a picture of the single-site hole localization. The paper is organized as follows. In Sec. II, we start by describing in detail the theoretical methodology employed. Sections III and IV analyze the structure and electronic levels of substitutional and interstitial Li. The formation energies of both defects are compared in Sec. V, where results are given both for O-rich and Zn-rich conditions. In Secs. VI A and VI B, we determine the activation energy for diffusion of interstitial Li and for the replacement of a Zn lattice atom by a Li atom, respectively. In light of the results of this study, Sec. VII provides a discussion concerning the use of Li as single *p*-type dopant in ZnO, Finally, the conclusions are summarized in Sec. VIII.

II. THEORETICAL METHOD

The present calculations are based on spin-polarized density functional theory. In order to address the band-gap problem we performed (i) first-principles calculations with a generalized gradient approximation (GGA) (Ref. 36) for the exchange and correlation energy (E_{xc}) and (ii) calculations employing a HDF based on the Perdew-Burke-Ernzerhof (PBE) approximation, obtained by replacing a fraction α of PBE exchange with Hartree-Fock exchange.[37] A factor $\alpha = 0.32$ was chosen to fit the Kohn-Sham band-gap energy of ZnO. The integrable divergence of the Hartree-Fock exchange term was treated explicitly.[38]

We also used pseudopotentials generated using two different schemes: a set of ultrasoft Vanderbilt (VDB) pseudopotentials and a set of norm-conserving Troullier-Martins (TM) pseudopotentials, for each of the three species considered (Zn, O, and Li).

The ZnO structural parameters obtained using both pseudopotential sets are in very good agreement with experiment (Table I). As expected, the Kohn-Sham band gap of ZnO, calculated using the semilocal density functional, is highly underestimated: 0.72 eV when the ultrasoft VDB pseudopotentials are used or 0.76 eV when the TM pseudopotentials are used. With the hybrid density functional tuned to open a gap of 3.42 eV at the Γ point, the valence- and conduction-band states are shifted, respectively, by −1.80 and 0.86 eV. We note that the comparison between the positions of the band edges for PBE and HDF requires the align-

TABLE I. Structural parameters and Kohn-Sham energy gap at Γ obtained using TM or VDB pseudopotentials, both employing the PBE functional. The parameter u refers to the relative displacement between anion and cation sublattices. The results were obtained using a primitive wurtzite cell with converged BZ sampling (MP-8^3). Experimental values (Ref. 1) are also given for comparison.

Pseudo.	a (Å)	c/a	u	E_g (eV)
TM	3.2880	1.606	0.379	0.76
VDB	3.2898	1.614	0.378	0.72
Expt.	3.2495	1.593–1.6035	0.3817–0.3856	3.44

ment of the electrostatic potentials in the two calculations.[39,40]

Calculations both with the VDB and TM pseudopotentials were performed using the QUANTUM-ESPRESSO and CPMD packages, respectively.[41,42] The calculation setups can be summarized as follows. First, the ultrasoft VDB pseudopotentials were used together with the generalized gradient approximation of Perdew, Burke, and Ernzerhof (PBE) for the E_{xc} functional, and a plane-wave basis set defined by a cutoff of 30 Ry. The Kohn-Sham states of the systems with unpaired electrons were filled using first-order Methfessel-Paxton smearing[43] with a small temperature (0.005–0.001 Ry). This faster calculational approach enabled us to perform geometry relaxations and saddle-point calculations using supercells of different sizes (32–192 atoms) and sampling the Brillouin zone (BZ) at multiple **k** points (following Monkhorst-Pack sampling schemes). These calculations will be noted by PBE-VDB.

On the other hand, we performed calculations employing the HDF for the exchange and correlation energy. The HDF calculations were performed using the norm-conserving TM pseudopotentials and a higher kinetic-energy cutoff of 100 Ry (except for full geometry optimizations at HDF level, with a cutoff of 80 Ry). We will thus label them HDF-TM. Due to the high computational effort associated with the HDF calculations, we had to adopt some further approximations. The BZ was sampled only at the Γ point, and, unless otherwise stated, the respective density and total energy were calculated using the relaxed structures obtained from the PBE-VDB calculations in a supercell of the same size.

Last, we also performed an additional set of calculations identical to HDF-TM with the only difference that the PBE functional was used instead (PBE-TM). The reason for repeating a number of calculations using the PBE functional is to make sure that the differences between PBE-VDB and HDF-TM calculations arise from the use of an improved exchange-correlation functional and not from the different pseudopotentials and basis sets.

The pseudopotentials used in all the calculations were generated for the PBE functional.

Formation energies

The formation energy of a defect or impurity X in charge state q, at a temperature $T=0$, is defined as

$$E_f[X^q] = E[\mathrm{Zn}_n\mathrm{O}_m{:}X^q] - \sum_i n_i\mu_i + q(E_F + E_v) + \delta\phi, \quad (1)$$

where $E[\mathrm{Zn}_n\mathrm{O}_m{:}X^q]$ is the energy of a $\mathrm{Zn}_n\mathrm{O}_m$ supercell containing the defect X, n_i is the number of atoms of species i in the supercell and μ_i is the respective chemical potential. Also $-q$ and (E_F+E_v) represent, respectively, the number of extra electrons in the supercell and their chemical potential. The Fermi level E_F is defined relative to the valence-band top E_v, which therefore is included explicitly in the calculation of the formation energies of charged defects. E_v is obtained from the bulk ZnO calculation and subsequently corrected for the different reference potentials in the bulk and defective supercells. This correction is performed by aligning the reference of the electrostatic potentials of the neutral defective supercell and of the bulk supercell using the average at an (0001) plane far from the defect.[44,45]

Corrections for finite system-size effects may also be included and we note them by $\delta\phi$. Apart from the potential alignment mentioned above which is also size dependent, different recipes have been proposed to correct for band-filling and artificial electrostatic interaction resulting from the periodic boundary conditions (including image-charge effects) but there is no unanimity about the quality of these corrections.[45–47] For example, the application of a correction for spurious electrostatic interaction as proposed by Makov and Payne[48] (herefrom referred to as electrostatic correction) has been object of debate and it has been argued that it significantly overestimates the error leading to inaccurate results specially in the case of delocalized defect states.[45,49,50] On the other hand, doubt has been cast over results of calculations of defect levels which did not account for finite-size effects.[47]

Discussing the validity of postprocessing correction schemes is not the aim of the present paper. It is generally accepted that the converged formation energy (in the $L\to\infty$ limit) lies between the uncorrected value ($\delta\phi=0$) and the upperbound defined by the first-order Makov-Payne correction ($\delta\phi=\Delta\phi_{\mathrm{MP}}$),[48] given by

$$\Delta\phi_{\mathrm{MP}} = \frac{q^2\alpha_M}{2\epsilon L}, \quad (2)$$

where ϵ and α_M are the dielectric permittivity and Madelung's constant, and L will be taken to be the cubic root of the supercell volume. We thus give both corrected and uncorrected values which indicate a range of confidence for the calculated results. Similarly, we do not apply a postprocessing band-filling correction for shallow levels but the finite-size effects are commented in the text when appropriate.

The chemical potentials are defined by the experimental growth conditions, which can range from Zn rich to O rich. They should therefore figure explicitly as variables in our formalism. However, it is useful to consider extreme conditions, which establish bounds for the chemical potentials of the elements and are useful to the interpretation of the results. For Zn-rich conditions, we assumed that ZnO is in contact with a reservoir of Zn in the metallic form whereas in O-rich conditions we assume that the material is in contact with molecular oxygen. Spin polarization was taken into ac-

count in the determination of the chemical potential of O from the oxygen molecule. For Li, we have assumed equilibrium with a bcc-Li phase since metallic precipitation is observed in Li oversaturated material.[27]

The use of a hybrid correction to the PBE E_{xc} functional shifts the valence-band states as well as the conduction-band states. This brings the band-gap energy closer to the correct value, simultaneously shifting the positions of defect energy levels with respect to the band edges. The more accurate treatment of the exchange interaction may also correct the absolute formation energies of some neutral defects. However, we will assume that the cohesive energies of the metallic systems, well described by PBE, do not change significantly. This approximation will be used to calculate the chemical potentials of the metals in the reference systems (bcc-Li and hcp-Zn).

The ionization levels $E(q/q+1)$ of defect and impurities can be found by determining the position of the Fermi level for which $E_f(q)$ equals $E_f(q+1)$. Ionization levels do not depend on the chemical potential of the atoms but only on the difference of the total energies of the defects in different charge states and on the position of the valence band.

III. SUBSTITUTIONAL Li

ZnO has a wurtzite structure (C_{6V}^6 or $P6_3mc$), defined by two lattice parameters a and c and the relative displacement of the Zn and O sublattices (u). Each Zn atom is tetrahedrally coordinated. In an ideal wurtzite structure, with $c/a=\sqrt{(8/3)}$ and $u=3/8$, the local environment of the Zn site is tetrahedral but ZnO crystals deviate from this arrangement having a longer Zn-O bond along the polar c axis.

Li can easily loose its valence electron and thus it prefers to sit on the cation site, where it substitutes for Zn. The zinc atom furnished two electrons to the O $2p$ states while Li can only provide its single $2s$ electron. Hence, the Li_{Zn} center is an acceptor. Li at the anion site (Li_O) is energetically unfavorable and can be disregarded.[26]

A. Structure

The results of a geometry optimization of the Li_{Zn}^0 structure using the PBE functional show very little displacement of the neighboring oxygen atoms [Fig. 1(a)]. In the negative charge state, the Li-O bonds are expanded by less than 0.2% compared to the bonds of the host crystal. The calculated bond lengths are 2.01 Å both for the axial and nonaxial bonds. In the negative charge state, these change by less then 0.01 Å. These results are in agreement with previous calculations.[12,26,30] The next Zn shell however relaxes inward leading to a small volume contraction of the solid.

Subsequently, we investigated the stability of a distorted structure where Li is displaced along the C_3 axis, elongating the axial Li-O bond. This perturbation of the structure is expected to stabilize the unpaired hole at the axial O site as observed experimentally.[19] However, we did not find an energy minimum of the PBE potential-energy surface which can describe this state. This is due to the self-interaction error inherent to the semilocal GGA approximation, which tends to overdelocalize the charge density.

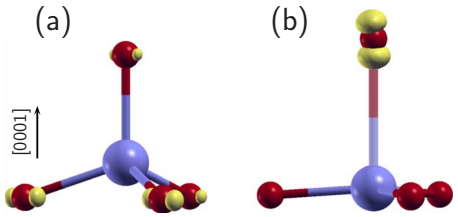

FIG. 1. (Color online) Isosurface of the spin density (Ref. 51) associated with the neutral Li_{Zn} defect, as calculated (a) with the PBE functional, for the centered PBE geometry, (b) with the HDF functional, for the off-centered HDF geometry (Ref. 52). For clarity, the charge density in (a) was multiplied by a factor of 2. Li and O atoms are represented by blue and red spheres, respectively, (gray and black, respectively, in the grayscale version), and the elongated bond is faded.

In contrast, the HDF model shows an off-center localized state. We performed a full structural optimization of a perturbed Li_{Zn} structure using the HDF for the exchange and correlation energy in a 32-atom supercell. This approach required a high computational effort, but is necessary because the distortion leads to a high localization of the unpaired electron level on one of the oxygen orbitals.[35] We obtain a stable off-centered structure, where the Li atom and the nearest O neighbor are displaced along the C_3 axis. The final positions are, respectively, 0.56 and 0.18 Å from the original sites of the undistorted structure, and the resulting Li-O bond is elongated by about 36%, [Fig. 1(a)], in good agreement with the results of EPR experiments suggesting an elongation of about 40%.[19]

In order to obtain more accurate total energies and electronic levels, the coordinates of the Li atom and its neighbors at the nearest anion and cation shells, obtained from the 32-atom supercell calculation, were embodied in a 72-atom supercell, and the atoms farther away from the defect were optimized at PBE level. Subsequently, the total energies were recalculated with the HDF. The off-centered structure was found to be a local potential energy minima, 0.28 eV higher in energy than the centered structure, in contrast with the EPR observations which suggest that the localized hole state is more stable. Despite the accurate description of the geometry of the defect, the HDF is not yet able to predict the small energies associated with the transition between localized and delocalized hole states, likely because the fraction of exact exchange that gives the right band gap is not enough to cancel completely the self-electron interaction.

B. Energy levels

At the PBE level, the electronic structure of Li_{Zn} is characteristic of a shallow acceptor center. The introduction of Li_{Zn} leaves empty a Kohn-Sham state lying in the top of the valence band. This perturbed host state has predominantly valence-band character and its dispersion is very similar to that of the uppermost valence band. The $E(-/0)$ level is about 0.1 eV from the valence-band top. Due to its shallow nature, the level position converges slowly with the size of the system, and with the number of **k** points used for BZ sampling (Fig. 2).

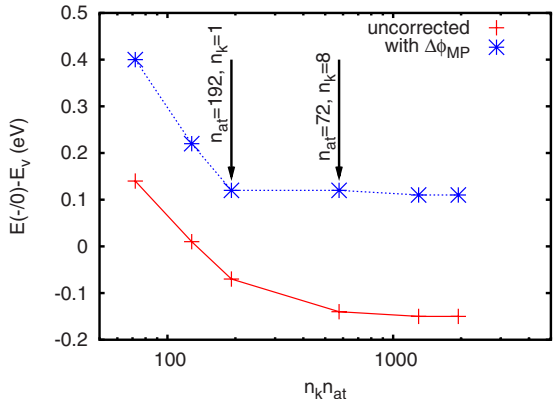

FIG. 2. (Color online) Convergence of the position of the Li_{Zn} $(-/0)$ level, obtained using the PBE functional and VDB pseudopotentials, with the number of atoms in the supercell (n_{at}) and the number of **k** points used for BZ sampling (n_k).

The principal sources of error associated with finite supercell size are band-filling and spurious electrostatic interaction effects. While the former increases the calculated energy of the neutral state, the latter lowers the energy of the negative charge state. Therefore, both contribute to the underestimation of the separation of the $(-/0)$ level from the valence-band top in small supercells.

We first consider the band-filling effects associated with the spurious dispersion of the defect state caused by defect-defect interaction. In a very large supercell, at very low defect concentration, the extra hole is at the top of the valence band (i.e., at the Γ point or the equivalent **k** points originated by the translational symmetry). However, in our finite-size supercells all inequivalent **k** points contribute to the energy of this hole according to their respective weights.[45,47] A careful convergence study shows that the level is already converged within 0.01 eV for a 72-atom supercell with $n_k=18$ or in a 192-atom supercell with $n_k=1$ (Fig. 2). We found that the postprocessing correction suggested by a recent work[47] overestimates the error, giving for $n_{at}=72$ and $n_k=8$ a shift of 0.24 eV, much larger than the error that can be estimated from the comparison with the results in the larger supercell.

On the other hand, the energy of the negative charge state is underestimated due to the interaction with the neutralizing background charge. Here we apply the Makov-Payne correction described in Sec. II, which in this case improves the convergence of the calculated ionization energies (Fig. 2).

Now it is important to understand if the shallow nature of the level is an intrinsic property of the defect or a side effect of a deficient description of the exchange-energy term. This issue is clarified by comparing the results of PBE and HDF calculations. The HDF treatment essentially affects the ionization energy of the system in two ways. First, by correcting the relative energy of filled and empty one-electron states; second, by changing the defect structure, introducing a state where not only the impurity but also one of the oxygen atoms are displaced off site. We discuss both effects separately.

Let us first consider the impact of the band-gap underestimation on the ionization energy of Li_{Zn}, by recalculating the $E(-/0)-E_v$ energy at the HDF level, using the geometry obtained from the PBE calculation. The alignment of the

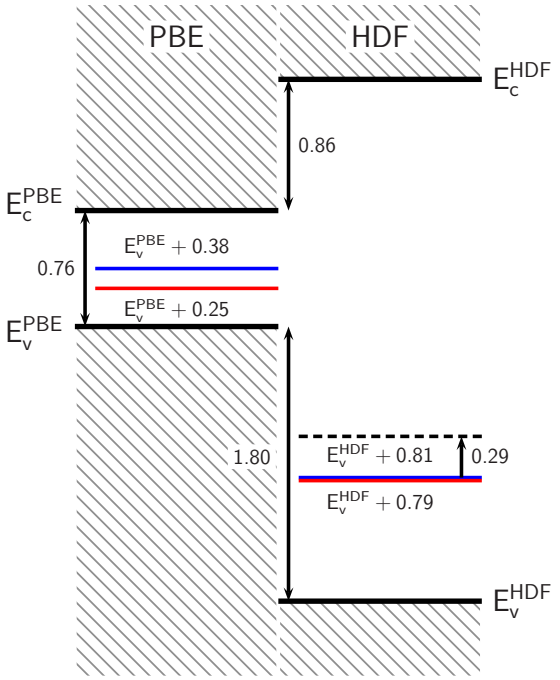

FIG. 3. (Color online) Position of the calculated $Li_{Zn}^{-/0}$ level (eV) with respect to the ZnO band edges, calculated using the PBE or the HDF, on a common energy scale obtained upon alignment of the electrostatic potential (Refs. 39 and 40). Levels in blue (dark gray) and red (light gray) were obtained, respectively, in supercells of 72 and 128 atoms. All values were obtained through Γ-point sampling and use of TM pseudopotentials and include Makov-Payne correction. The dashed line indicates the deviation of the level if relaxation effects are calculated at HDF level.

electrostatic potential in the PBE and HDF calculations allows the comparison of the energy levels obtained using the two schemes on a common energy scale.[39,40] The acceptor level, arising from a perturbed valence-band state, is shifted away from the valence-band edge when the band gap is opened by applying the HDF scheme. The resulting $E(-/0)=E_v+0.79$ eV level (where an electrostatic correction of 0.26 eV has been included) is shifted down by about 1.2 eV relative to the PBE level calculated in the same conditions (Fig. 3). With the HDF, the charge density of the unpaired electron becomes more localized (Fig. 1), and $E(-/0)$ is less dependent on the system size. As shown in Fig. 3, the levels calculated in supercells of 72 and 128 atoms are practically coincident.

Let us now turn on the influence of the atomic displacements to the ionization level. The ionization energies were recalculated using the defect geometries optimized at the HDF level, using the methodology described in the previous section. As expected, the relaxation of the centered structures of the neutral and negatively charged defects changes little the transition level, bringing it 0.29 eV deeper than in the HDF calculation based on the on-centered PBE structures (Fig. 4). However, we recognize the off-centered structure, observed experimentally, as the true ground state of the neutral defect. In our HDF calculation, the $(-/0)$ level of the off-centered defect is only 0.01 eV above the $(-/0)$ level obtained for the PBE geometries. As α is increased further,

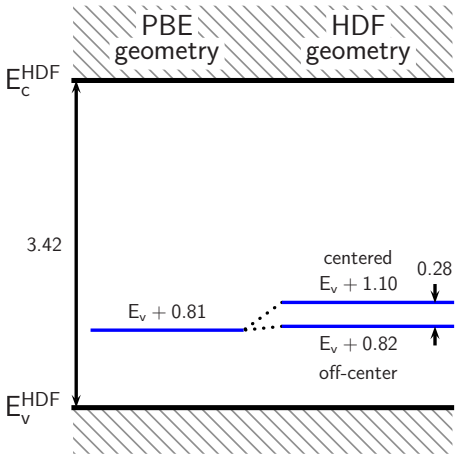

FIG. 4. (Color online) Influence of the functional used for geometry optimization on the position of the calculated $Li_{Zn}^{-/0}$ level. The level on the left was obtained from HDF total-energy calculations for the structures obtained from the PBE relaxation. The levels on the right were obtained from HDF calculations of the centered and off-centered defect geometries calculated with the HDF. All values (eV) were obtained in 72-atom supercells, through Γ-point sampling and use of TM pseudopotentials.

we expect that the energy of the off-centered structure will become lower in energy with respect to the centered structure. Hence, it is reasonable to assume that at the current value of α (0.32), the energy of the off-centered structure is being overestimated. Using the energy of the off-centered structure calculated in the HDF approach, this allows us to obtain a lower bound for $E(-/0)$ at $E_v+0.82$ eV.

Thus, taking into account both the uncertainty arising from finite supercell size effects (including spurious electrostatic effects) and hole localization effects, we place the $(-/0)$ level of Li_{Zn} no lower than $E_v+0.6$ eV. This result is closer to the the "deep" Li acceptor of Refs. 15, 22, and 23 than to the "shallow" Li acceptor of Refs. 14 and 16–18 (Table II).

IV. INTERSTITIAL Li

Alternatively, Li may reside at an interstitial site. In the interstitial form Li readily looses its outmost electron behaving as a shallow donor.[26] We investigated different defect geometries. In the most relevant, stable configurations, Li occupies the empty cages of the wurtzite structure, either at the octahedral (O) or at the tetrahedral (T) interstitial site (Fig. 5).

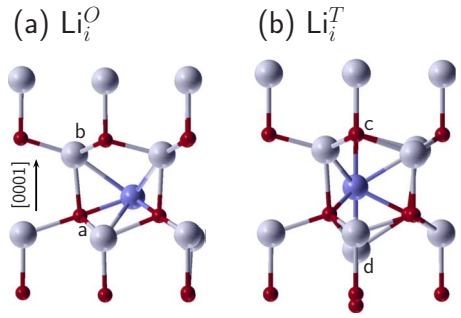

FIG. 5. (Color online) Geometry of interstitial Li (a) at the octahedral interstitial site and (b) at the tetrahedral interstitial site. Li atoms are represented by blue (gray) spheres while O and Zn atoms are represented by red (black) and white spheres, respectively.

We start by considering the relative energies of the different sites in the positive charge state. The most stable configuration is at the O site (Li_i^O) where Li is 0.62 eV lower in energy than at the T site (Table III).[26,29] When placed in the octahedral cage, the Li atom is slightly displaced along the [0001] toward the neighboring oxygen atoms, similar to what has been found for the zinc interstitial (Zn_i).[6] Similarly, in the T configuration, Li is closer to the oxygen atom, repelling the zinc. We also found a local minimum similar to Li_i^O, where both the Li and its closest Zn neighbor (labeled Zn_e in Fig. 5) are slightly displaced from the trigonal axis, which we label Li_i^{T*} but this structure is only marginally stable, separated from Li_i^T by a barrier of about 0.02 eV. We also investigated Li_{Zn}-Zn_i pairs and interstitialcies with different orientations but all of them spontaneously transform into Li_i^O, Li_i^T, or Li_i^{T*}.

The effect of adding an electron to the supercell containing $\{Li_i^O\}^+$ or $\{Li_i^O\}^0$ corresponds to placing an extra electron in a conduction-band state. Thus in the PBE calculations,

$$E_{Li_i^O}^{0/+1} = E[Zn_nO_n{:}Li_i^0] - E[Zn_nO_n{:}Li_i^{+1}] - E_v$$

equals the position of the quasiparticle conduction band calculated in the bulk supercell. The same result is obtained if

TABLE II. Position of the $Li_{Zn}^{-/0}$ level with respect to E_v calculated using different pseudopotentials and E_{xc} functionals. Values outside (inside) brackets were obtained in supercells of 72 (128) atoms. The largest shift of the level position when relaxation effects are taken into account is represented as a dashed line in Fig. 3 (see text). Experimentally the ionization energies are 100–300 meV for the shallow Li acceptor (Refs. 14 and 16–18) and above 600 meV for the deep Li acceptor (Refs. 15, 22, and 23). All calculations were performed at the and Γ point.

Pseudopotential	E_{xc}	$E(-/0)$	$E(-/0)$ with $\Delta\phi_{MP}$
VDB	PBE	0.14(0.01)	0.40(0.22)
TM	PBE	0.12(0.04)	0.38(0.25)
TM	HDF	0.55(0.58)	0.81(0.79)

TABLE III. Formation energies (eV) of different configurations of positively charged Li_i, for Zn-rich material and $E_F=E_v$. The values were obtained with $n_{at}=72$ and $n_k=8$, using VDB pseudopotentials and the PBE functional. Energies obtained using the TM pseudopotentials are given in brackets.

Defect	E_f	E_f with $\Delta\phi_{MP}$
Li_i^O	−2.09(−1.92)	−1.83(−1.66)
Li_i^T	−1.47	−1.21
$Li_i^{T,*}$	−1.46	−1.20

the band gap is opened, shifting up the conduction-band states.

Since the defect is always positively charged, the PBE approach already provides a good description of the system. Thus, the geometry and relative energies between the equilibrium points change little in HDF calculations. This is confirmed by test calculations for substitutional Li involving a full structural relaxation of Li_i^O and Li_i^T at the HDF level using 32-atom supercells, similar to those reported in Sec. III, yielding a relative energy of 0.83 or 0.09 eV higher than the result of a similar calculation at the PBE level. This difference is comparable with, for example, those arising from the use of different pseudopotentials (~0.1 eV).

V. FORMATION ENERGIES

The populations of the two fundamental forms of Li in ZnO, Li_{Zn} and Li_i^O, will result from the equilibrium between the reactions of cation defects (Li_{Zn}, Zn_i, V_{Zn},…), precipitation of Li and surface oxidation, under the constraints imposed by charge neutrality.

Since the formation energies of both defects—charged over a wide range of Fermi energies—depend explicitly on the position of E_F with respect to the band edges, the band-gap error has a critical impact on the determination of their relative stabilities. The formation energies of the substitutional and interstitial species, calculated using PBE and HDF are plotted in Fig. 6 for the two limiting scenarios: O-rich and Zn-rich conditions. On a common energy scale (obtained upon alignment of the electrostatic potentials in the two calculations) the formation energies of Li_{Zn}^- and $\{Li_i^O\}^+$ remain practically unchanged with the introduction of a fraction of exact exchange. In contrast, the formation energy of neutral Li_{Zn}, with an unpaired electron in its perturbed valence-band state, is raised by about 1 eV.

However, the major change is the opening of the window of accessible Fermi energies. The HDF results show that even in O-rich material, below $\simeq E_v + 1.8$ eV, Li_i^+ becomes more stable than Li_{Zn}^0, as opposed to what is observed in the narrow range defined by the PBE band gap. In Zn-rich material, Li_i^+ is expected to be always present in larger concentrations regardless of the conduction type. This explains the difficulties experimented in doping ZnO with this element.

In a material where Li defects are the dominant electrically active centers, the conduction type and carrier concentration will be determined by the ratio between the concentrations of Li_i and Li_{Zn}. The release of free electrons by ionized Li_i species enhances the stability of Li_{Zn} while the presence of the latter lowers the Fermi level favoring the formation of Li_i. Thus, even in O-rich material, there will always be self-compensation, pinning the Fermi energy above the acceptor level of Li_{Zn}.

VI. DIFFUSION

A. Interstitial migration

It was shown in the previous sections that in Zn-rich and *p*-type O-rich material, Li is most stable as an interstitial impurity. It is a fast diffusing element since it can migrate

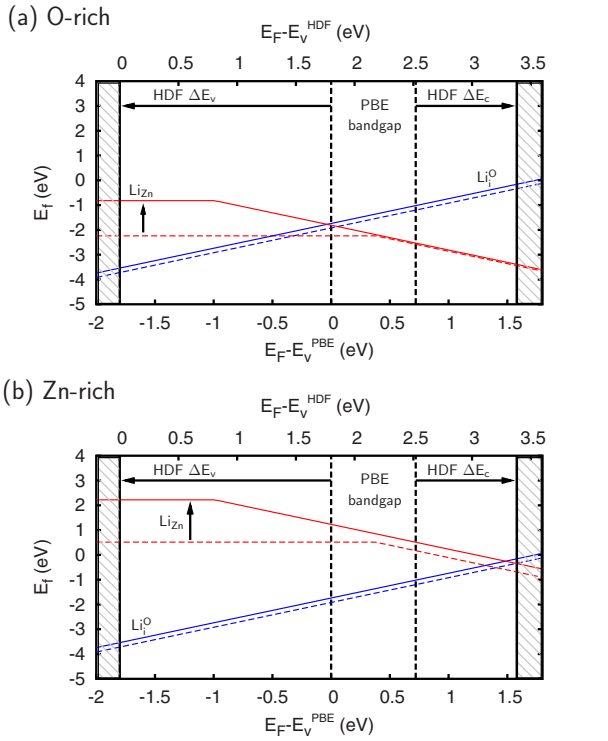

FIG. 6. (Color online) Formation energies of Li defects (a) in O-rich conditions and (b) Zn-rich conditions. PBE and HDF results are represented by dashed and full lines, respectively. The shifts of the band edges and formation energies of the neutral defects with the partial introduction of exact Hartree-Fock exchange (from the HDF calculation) are indicated with arrows.

through the open channels of the wurtzite lattice. Axial diffusion through the ⟨0001⟩ trigonal channels requires little displacement of the host atoms and minimizes the ionic repulsion along the path. Nevertheless, diffusion in the perpendicular direction (basal diffusion) also requires a low activation energy, as the defect exploits the passage through the metastable *T* sites when jumping between octahedral cages.

The respective minimum-energy paths for the migration both along the axial direction and on the basal plane were investigated with recourse to the nudged elastic band (NEB) method.[53] A linear interpolation of the initial and final positions was used as a start. The image highest in energy was allowed to climb along the path in order to find the saddle point. The defect was positively charged.

The migration along the axial direction is straightforward. Both the equilibrium and saddle positions are at the center of the channel. Two equivalent *O* sites aligned along the [0001] direction are separated by a potential-energy barrier of 0.7 eV. The saddle is reached when the Li atom passes through the puckered hexagonal site, more exactly at the center of a triangle of Zn atoms. This is in good agreement with a previous study.[26]

To diffuse in the basal plane, the defect has to jump between octahedral cages at different [0001] channels. The existence of a low-energy metastable position for Li_i at the *T* site, only 0.62 eV higher in energy, facilitates this process. Only a little extra activation energy is necessary to activate the transition. Migration via $Li_i^O \rightarrow Li_i^T \rightarrow Li_i^{O'}$ jumps, re-

TABLE IV. Activation energies (eV) for diffusion of Li_i^+ calculated through the use of VDB or TM pseudopotentials, MP-2[3] or Γ-point sampling, and PBE or HDF functionals for the exchange energy (see text). The barriers are measured from the absolute energy minimum (at the *O* site).

			$Li_i^O \rightarrow Li_i^T$	$Li_i^O \rightarrow {}^aLi_i^{O'}$
Pseudopotential	E_{xc}	n_k	Basal	Axial
VDB	PBE	8	0.66	0.67
VDB	PBE	1	0.66	0.66
TM	PBE	1	0.79	0.71
TM	HDF	1	0.82	0.73

quires an activation energy of 0.6–0.7 eV, very close to the axial migration barrier (Table IV). However, the trajectory is zigzag fashioned rather than straight as along the axial direction. The pseudopotential/cutoff combination employed in the calculation has a small impact on the energy barriers (Table IV).

Since there is no change in the charge state of the defect along the trajectory, the choice of exchange functional does not have a critical influence on the energy profile, and relative energies are little affected by the band-gap error. This is attested by the activation energies calculated at the HDF level for the saddle-point coordinates obtained at PBE level (Table IV).

The calculated energy barrier is lower than the measured activation energy (0.98 eV) figuring in the diffusion constant of interstitial Li between 500 and 700 K $D=0.020 \times \exp(-0.98\ \text{eV}/kT)\ \text{cm}^2\ \text{s}^{-1}$.[27] The difference may be justified by the presence of interacting defects and meddling of competing reactions.

B. Mechanisms of Li↔Zn replacement

In *n*-type O-rich material under thermodynamic equilibrium (E_F above $\sim E_v+1.8$ eV), Li_{Zn} becomes more stable than Li_i. Still, the low energy required for migration through the interstitial chains suggests that the interstitial species may still play the principal role in the diffusion. This requires the exchange between Li atoms at substitutional and interstitial sites, resulting from a reaction of replacement of Li by Zn or by a vacancy. We envisage two possibilities: (i) a kick-out mechanism,

$$Li_{Zn} + Zn_i \rightarrow Li_i \tag{3}$$

or (ii) a dissociative (Frank-Turnbull) mechanism,

$$Li_{Zn} \rightarrow Li_i + V_{Zn}. \tag{4}$$

Exchange mechanisms involving antisites require very high activation energies and can be discarded. Also an interstitialcy mechanism ($Li_{Zn}+Zn_i \rightarrow Li_{Zn}Zn_i$) is not possible since we did not find a stable interstitialcy.

The conditions in which an interstitial-mediated or vacancy-mediated diffusion mechanism will dominate are determined by the respective activation energies. We will compare the total activation energy necessary, in each case, to displace a Li_{Zn} defect to the interstitial site, via interaction with an intrinsic defect, and then reverse the reaction by returning Li to an equivalent Li_{Zn} position. The following analysis will be based on the formation energies obtained from the TM-HDF calculations, and we will use in first instance the results obtained after correcting for artificial electrostatic effects (the impact of $\delta\phi$ will be discussed afterward).

1. Activation energy for the kick-out mechanism

To obtain the activation energy for the transport of Li_{Zn} to a distinct substitutional site, we need to consider (i) the dominant barrier associated either with the direct kick-out reaction ("→") or the reverse transformation ("←") and (ii) the energy necessary to provide the zinc interstitial.

The zinc interstitial is always in the double positive charge state.[6,54] Thus, in the scenario of interest (O-rich, intrinsic, or *n*-type material) the kick-out reaction proceeds without capture or release of free-charge carriers,

$$Zn_i^{2+} + Li_{Zn}^- \rightarrow Li_i^+. \tag{5}$$

The associated exchange enthalpy is therefore independent of the Fermi level, as

$$\Delta H_{\text{kick}} = E_f(Li_i^+) - [E_f(Li_{Zn}^-) + E_f(Zn_i^{2+})]. \tag{6}$$

The calculations show that reaction (5) is exoenthalpic, with $\Delta H_{\text{kick}}=-2.76$ eV.

In view of this, Li_{Zn}^- are attractive sinks for free Zn interstitials. Nevertheless, thermal energy has to be provided to move them up to the vicinity of Li_{Zn}^- and power the kick-out reaction. The activation energy for migration of Zn_i^{++} [$W_{\text{mig}}(Zn_i^{++})$] is very low (about 0.6–0.8 eV according to Ref. 6) and only slightly anisotropic. However, the jump barrier varies with the distance to Li_{Zn}^-. The last barrier it encounters just as it nudges Li off the site will be noted $W_{\text{kick}}^{\text{I}}$.

We verify that $W_{\text{kick}}^{\text{I}}$ does not differ much from $W_{\text{mig}}(Zn_i^{++})$ by calculating the saddle-point energy for a kick-out path along the axial chain, represented in Fig. 7. The system was in the single positive charge state. The saddle point [Fig. 7(b)] occurs at the hexagonal site and is 0.78 eV higher in energy than the starting equilibrium point shown in Fig. 7(a), where the defects are ~4 Å apart. Obviously the kick-out path is not unique but by analogy with the migration of Zn_i we do not expect great anisotropy of the activation energies. It is thus reasonable to use $W_{\text{mig}}(Zn_i^{++}) \sim 0.8$ eV as an estimate.

The enthalpy of formation of the zinc interstitial necessary to trigger the kick-out reaction depends both on the Zn chemical potential and on the Fermi level (Fig. 9). In the O-rich limit, we obtain $E_f(Zn_i^{++})=0.73+2(E_F-E_v)$. Hence, in the E_F range of interest ($E_F > E_v+1.8$ eV), the energy necessary to provide Zn_i^{++} is larger than the energy released by the kick-out reaction, i.e., $E_f(Zn_i^{++}) > |\Delta H_{\text{kick}}|$ (Fig. 8). The dominant activation energy for the migration of Li via a kick-out mechanism, leaving the impurity back in a substitutional cation site, is

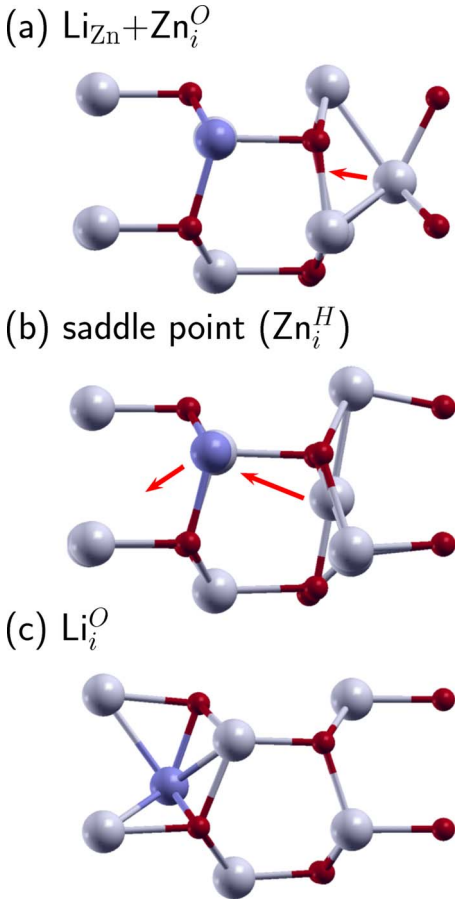

FIG. 7. (Color online) A $Zn_i^{2+}+Li_{Zn}^{-}\rightarrow Li_i^{+}$ kick-out reaction along the axial chain. Li atoms are represented by blue (gray) spheres while O and Zn atoms are represented by red (black) and white spheres, respectively. Arrows indicate the movement of the atoms.

$$W_{\mathrm{kick}} \simeq E_f(\mathrm{Zn}_i^{++}) + W_{\mathrm{mig}}(\mathrm{Zn}_i^{++}). \tag{7}$$

2. Activation energy for the vacancy-assisted dissociation mechanism

We now consider that Li_i is produced by the dissociation of Li_{Zn} [reaction (4)]. The return of Li to the substitutional site, eventually after a few migration steps, is assured by the recombination with a Zn vacancy [the reverse of reaction (4)]. From an energetic point of view, it is indifferent if Li_i recombines with the original vacancy at a distinct site (correlated pair recombination) or with another Zn vacancy (uncorrelated pair recombination).

As for the kick-out mechanism, we will find that the properties of the intrinsic defect mediating the replacement process are preponderant, and therefore we need to obtain reliable data for V_{Zn}. It is generally believed that this defect is a double acceptor, as expected from a simple ionic picture. However, the errors associated with spurious electrostatic effects, band-gap underestimation and self-interaction often have a great impact in the calculation of the $E(=/-)$ and $E(-/0)$ levels of this defect, justifying the spread of values in the literature.[4,6,10,54,55] Within the HDF framework, we obtain

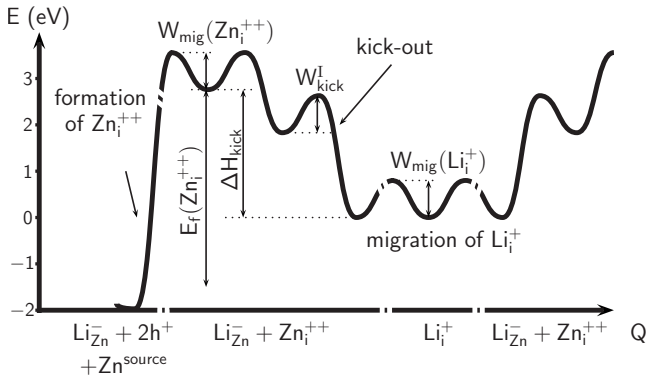

FIG. 8. A schematic potential-energy profile associated with the Zn-interstitial-mediated diffusion of Li_{Zn} via a kick-out mechanism. For illustration purposes, E_F was taken to be $E_v+2.0$ eV. Q represents a generalized coordinate.

$E(=/-)=E_v+1.80$ eV and $E(-/0)=E_v+0.62$ eV (Fig. 9). These are in good agreement with a recent study[54] and consistent with magnetic-resonance data.[56]

We start by evaluating the energy balance of the dissociation in the region defined by $E_F>E(V_{Zn}^{=/-})$, where the defects present before and after reaction (4) have the same number of electrons,

$$Li_{Zn}^{-} \rightarrow Li_i^{+} + V_{Zn}^{=}. \tag{8}$$

The respective dissociation enthalpy is

$$\Delta H_{\mathrm{diss}}^{=} = E_f(V_{Zn}^{=}) + E_f(\{Li_i^O\}^{+}) - E_f(Li_{Zn}^{-}) = 3.57 \text{ eV}. \tag{9}$$

The reaction is endoenthalpic in this direction, and the amount of energy transferred is larger than found for the kick-out mechanism.

There is an additional energy barrier associated with the liberation of Li from $V_{Zn}^{=}$. The barrier height was inspected by calculating the activation energy necessary to remove Li from a substitutional site and place it about 6.4 Å away from it.[57] The system had a total charge $q=-1$. The first step of Li_i^{+} toward dissociation involves overcoming a 0.44 eV energy barrier. We also considered an alternative dissociation path leading to an identical final state but involving predominantly the motion of $V_{Zn}^{=}$ but this requires a higher activation energy (0.71 eV). Both are less than the migration energies of the free defects [0.6–0.7 eV for Li_i^{+} and 1.0 eV for $V_{Zn}^{=}$ (Ref. 58)].

To complete the diffusion process, returning Li_{Zn} to a substitutional site different from the one where it started, it is required that V_{Zn} moves or a different vacancy is provided. Hence, in addition to the dissociation enthalpy, the migration energy of V_{Zn} has to be accounted for (Fig. 10). The overall activation energy is then

$$W_{\mathrm{diss}}^{=} \simeq |\Delta H_{\mathrm{diss}}^{=}| + W_{\mathrm{mig}}(V_{Zn}^{=}) = 4.57 \text{ eV}. \tag{10}$$

For $E(Li_{Zn}^{-/0})<E_F<E(V_{Zn}^{=/-})$ (approximately between $E_v+0.8$ eV and $E_v+1.8$ eV), the dissociation and recombination involve a capture or release of a free hole,

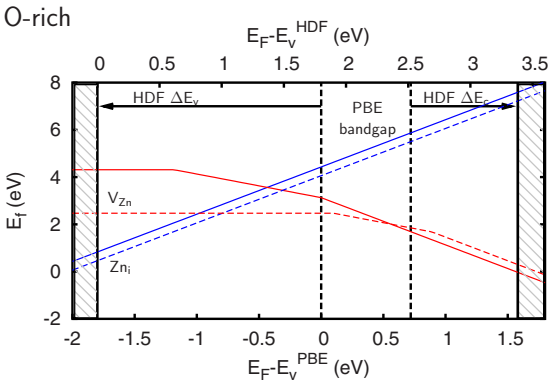

FIG. 9. (Color online) Formation energies of the zinc vacancy and zinc interstitial in O-rich conditions. Dashed and full lines represent PBE and HDF results, respectively. The results were obtained in 72-atom supercells, through Γ-point sampling and TM pseudopotentials, and include Makov-Payne corrections.

$$\mathrm{Li}_{\mathrm{Zn}}^{-} \rightarrow \mathrm{Li}_{i}^{+} + \mathrm{V}_{\mathrm{Zn}}^{-} - \mathrm{h}^{+}. \tag{11}$$

For the forward reaction, the enthalpy change will be lower,

$$\Delta H_{\mathrm{diss}}^{-} = \Delta H_{\mathrm{diss}}^{=} - [E(\mathrm{V}_{\mathrm{Zn}}^{=/-}) - E_F] \tag{12}$$

while the reverse reaction is still exoenthalpic. The migration energy is also slightly higher in the single negative charge $[W_{\mathrm{mig}}(\mathrm{V}_{\mathrm{Zn}}^{-})=1.1$ eV according to Ref. 58]. The activation energy for the Frank-Turnbull mechanism in the region of stability of $\mathrm{V}_{\mathrm{Zn}}^{-}$ is then

$$W_{\mathrm{diss}}^{-} = \Delta H_{\mathrm{diss}}^{=} - [E(\mathrm{V}_{\mathrm{Zn}}^{=/-}) - E_F] + W_{\mathrm{mig}}(\mathrm{V}_{\mathrm{Zn}}^{-}), \tag{13}$$

slightly lower than in the $E_F > E(\mathrm{V}_{\mathrm{Zn}}^{=/-})$ regime, and depending explicitly on the Fermi level.

The activation energies for the kick-out and dissociation mechanisms are plotted in Fig. 11 for the O-rich limit. In such conditions (and within the Fermi energy range defined by $E_F < \mathrm{Li}_{\mathrm{Zn}}^{-/0}$), the dissociative diffusion mechanism dominates. The dominant factor determining the Li↔Zn replacement mechanism is the energy necessary to create the intrinsic defect that acts as a mediator.

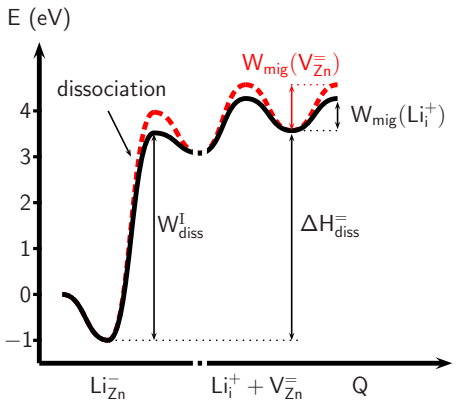

FIG. 10. (Color online) A schematic potential-energy profile associated with the Zn-vacancy-mediated diffusion of $\mathrm{Li}_{\mathrm{Zn}}$ via a dissociative mechanism. The profile drawn in black represents the motion of Li away from the vacancy (following the breakup) whereas the profile in red (gray) represents the motion of the vacancy away from Li. Q is a generalized coordinate.

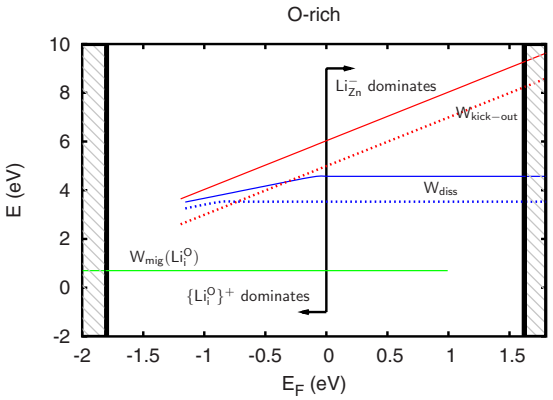

FIG. 11. (Color online) Comparison of the energy necessary to activate different mechanisms of Li diffusion in O-rich conditions, as a function of the Fermi level. The results are based on calculations carried out in 72-atom supercells, with the HDF approximation for the exchange functional. For W_{diss} and W_{kick}, filled and dotted lines represent, respectively, the results with and without electrostatic correction.

Thus, if μ_{O} is slightly lower than in the extreme O-rich setting, kick-out diffusion, mediated by the Zn interstitial, becomes more favorable in the intrinsic material. However, the range of E_F where $\mathrm{Li}_{\mathrm{Zn}}$ dominates over Li_i is also confined to a region closer to the conduction band. The kick-out process will have an important contribution out of thermodynamic equilibrium, if the material is oversaturated with Zn interstitials.

Both mechanisms involve doubly charged defects, whose formation energies are affected by spurious electrostatic interactions, including image-charge effects. Nevertheless, as can be noticed in Fig. 11, the Makov-Payne correction shifts equally $\Delta H_{\text{kick-out}}$ and $\Delta H_{\mathrm{diss}}^{=}$ and thus does not affect the comparison between the two mechanisms.

VII. Li AS A *p*-TYPE DOPANT

The detailed analysis presented so far enables us to evaluate the possibilities of Li as a single *p*-type dopant. We discuss four fields where limitations might arise.

A. Solubility

Following our detailed investigation of the dependence of the formation energy of $\mathrm{Li}_{\mathrm{Zn}}$ on the atomic potentials, it is evident that the substitutional solubility can be enhanced significatively with a careful choice of precursors and growth conditions. In the optimal conditions where $2\mu_O = E(\mathrm{O}_2)$ and $\mu_{\mathrm{Li}} = E(\mathrm{Li}^{\mathrm{bcc}})$, the formation energy of $\mathrm{Li}_{\mathrm{Zn}}$ is actually negative across the whole band gap (ranging between −1.8 and −4.2 eV). This means that the transfer of a Li atom from a reservoir in the metallic phase to a substitutional site in ZnO, accompanied by the oxidation of a Zn atom at the surface lowers the energy of the system.

B. Self-compensation

The limitations associated with the dependence of $E_f(\mathrm{Li_{Zn}})$ on the Fermi level are more difficult to overcome. The negatively charged defects have a higher energy in p-type material. The problem is that as the concentration of ionized $\mathrm{Li_{Zn}}$ increases, the Fermi energy moves toward E_v, increasing its formation energy and at the same time decreasing the formation energy of $\{\mathrm{Li}_i^O\}^+$, which act as compensating centers. The ratio between the concentrations of the two species will result from a delicate equilibrium between free carriers, Li defects and intrinsic defects. In essence, this places a limit to the free-hole density that can be achieved. According to the "doping pinning rule", the lower the VBM of a semiconductor, the lower its p-type dopability.[59] ZnO, with the lowest E_v among the most used II-VI semiconductors, is a critical case.

C. Ionization energy

The acceptor activation rate will depend not only on the fraction of Li at the substitutional sites but also on the efficiency of ionization at operating temperature. Shallow defects are promptly ionized at room temperature but if the impurity level is 0.6–1.1 eV above the valence-band top, it is unlikely able to provide the free-hole density required for electronic applications. This seems to be the case of $\mathrm{Li_{Zn}}$, as the hybrid density functional calculations have revealed that its $(-/0)$ level does not shift together with the valence-band states where it originates from. Increasing the fraction of exact exchange, the lowest-unoccupied state of $\mathrm{Li}_{\mathrm{Zn}}^0$ becomes more localized and the ionization energy of $\mathrm{Li}_{\mathrm{Zn}}^-$ is raised to 0.8 eV—rather than the <0.1 eV resulting from the PBE calculation.

D. Stability face to diffusion-limited reactions

A point in favor of $\mathrm{Li_{Zn}}$ is that, once the conditions of formation are met, it is likely to remain up to higher temperatures than the competing interstitial species. In fact, whereas Li_i migrates with an activation energy as low as 0.7 eV, being easily trapped at other defects, once incorporated at the substitutional site Li becomes remarkably stable. The dissociation energy is about 4 eV and kick-out by a Zn_i becomes unlikely in O-rich material, where the formation energy of the latter is rather high. This means that after an annealing treatment in an oxidizing atmosphere, if the equilibrium suffers a perturbation leading to a slight decrease in E_F and μ_{O}, $\mathrm{Li_{Zn}}$ will be preserved by a reasonably high kinetic-energy barrier. Nevertheless, its stability does not protect $\mathrm{Li_{Zn}}$ against the pairing with more mobile defects, among which Li_i, with opposite charge, is a major threat.

VIII. SUMMARY

We have performed a detailed density functional study of the formation energies, energy levels, and diffusion of substitutional and interstitial Li defects in ZnO. Calculations using a semilocal density functional yield that $\mathrm{Li_{Zn}}$ is a shallow acceptor with a $-/0$ level within 0.1 eV from the valence-band edge. However, when a hybrid density functional is used to open the band gap, its $-/0$ level moves away from the valence band. Taking into account both supercell size effects and relaxation effects, we place this level between 0.6 and 1.1 eV from the valence-band top, much deeper than indicated by the PBE calculations. Interstitial lithium is a shallow donor with its $(0/+)$ level resonant or very close to the conduction band.

Interstitial Li is very mobile, diffusing with an activation energy of 0.66–0.82 eV both in the axial plane and in the basal plane. This suggests that interstitial migration is the main vehicle of diffusion of Li. The replacement of Zn by Li and the reverse, resulting in the transport of $\mathrm{Li_{Zn}}$, can occur through a kick-out or a dissociative mechanism. The kick-out mechanism requires the lowest activation energy in Zn-rich material. In O-rich material, this mechanism is still preferred in p-type material. The dissociative mechanism is expected to dominate in n-type material.

ACKNOWLEDGMENTS

A.C. is thankful to DIT-EPFL for technical support to the use of the computing facilities Mizar, Alcor, and Bluegene. This work was supported by Swiss National Science Foundation.

[1] *Zinc Oxide Bulk, Thin Films and Nanostructures*, edited by C. Jagadish and S. J. Pearton (Elsevier, Amsterdam, 2007).
[2] A. Onodera, Ferroelectrics **267**, 131 (2002).
[3] P. Erhart, A. Klein, and K. Albe, Phys. Rev. B **72**, 085213 (2005).
[4] A. F. Kohan, G. Ceder, D. Morgan, and Chris G. Van de Walle, Phys. Rev. B **61**, 15019 (2000).
[5] S. B. Zhang, S.-H. Wei, and A. Zunger, Phys. Rev. B **63**, 075205 (2001).
[6] A. Janotti and C. G. Van de Walle, Phys. Rev. B **76**, 165202 (2007).
[7] S. Lany and A. Zunger, Phys. Rev. B **72**, 035215 (2005).
[8] S. Lany and A. Zunger, Phys. Rev. Lett. **98**, 045501 (2007).
[9] A. Janotti and C. G. Van de Walle, Appl. Phys. Lett. **87**, 122102 (2005).
[10] P. Erhart, K. Albe, and A. Klein, Phys. Rev. B **73**, 205203 (2006).
[11] F. Oba, A. Togo, I. Tanaka, J. Paier, and G. Kresse, Phys. Rev. B **77**, 245202 (2008).
[12] C. H. Park, S. B. Zhang, and S.-H. Wei, Phys. Rev. B **66**, 073202 (2002).
[13] Y. J. Zeng, Z. Z. Ye, W. Z. Xu, D. Y. Li, J. G. Lu, L. P. Zhu, and B. H. Zhao, Appl. Phys. Lett. **88**, 062107 (2006).
[14] Y. J. Zeng, Z. Z. Ye, J. G. Lu, W. Z. Xu, L. P. Zhu, B. H. Zhao, and S. Limpijumnong, Appl. Phys. Lett. **89**, 042106 (2006).
[15] B. K. Meyer, H. Alves, D. M. Hofmann, W. Kriegsies, D. For-

ster, F. Bertram, J. Christen, A. Hoffmann, M. Strassburg, M. Dworzak, U. Haboeck, and A. V. Rodina, Phys. Status Solidi B **241**, 231 (2004).
[16] O. Lopatiuk, L. Chernyak, A. Osinsky, and J. Q. Xie, Appl. Phys. Lett. **87**, 214110 (2005).
[17] B. Meyer, N. Volbers, A. Zeuner, S. Lautenschl ager, J. Sann, A. Hoffmann, and U. Haboeck, Mater. Res. Soc. Symp. Proc. Vol. 891 (Materials Research Society, Pittsburgh, 2006), p. EE10.
[18] X. H. Wang, B. Yao, Z. Z. Zhang, B. H. Li, Z. P. Wei, D. Z. Shen, Y. M. Lu, and X. W. Fan, Semicond. Sci. Technol. **21**, 494 (2006).
[19] O. F. Schirmer, J. Phys. Chem. Solids **29**, 1407 (1968).
[20] P. H. Kasai, Phys. Rev. **130**, 989 (1963).
[21] N. Y. Garces, L. Wang, N. C. Giles, L. E. Halliburton, D. C. Look, and D. C. Reynolds, J. Electron. Mater. **32**, 766 (2007).
[22] B. Meyer, J. Sann, and A. Zeuner, Superlattices Microstruct. **38**, 344 (2005).
[23] J. Sann, A. Hofstaetter, D. Pfisterer, J. Stehr, and B. K. Meyer, Phys. Status Solidi C **3**, 952 (2006).
[24] D. Zwingel and F. Gärtner, Solid State Commun. **14**, 45 (1974).
[25] A. R. Hutson, Phys. Rev. **108**, 222 (1957).
[26] M. G. Wardle, J. P. Goss, and P. R. Briddon, Phys. Rev. B **71**, 155205 (2005).
[27] J. J. Lander, J. Phys. Chem. Solids **15**, 324 (1960).
[28] S. B. Orlinskii, J. Schmidt, P. G. Baranov, D. M. Hofmann, C. de Mello Donegá, and A. Meijerink, Phys. Rev. Lett. **92**, 047603 (2004).
[29] E.-C. Lee and K. J. Chang, Phys. Rev. B **70**, 115210 (2004).
[30] J. Hu and B. C. Pan, J. Chem. Phys. **129**, 154706 (2008).
[31] S. Lany and A. Zunger, Phys. Rev. B **80**, 085202 (2009).
[32] O. F. Schirmer, J. Phys.: Condens. Matter **18**, R667 (2006).
[33] A. L. Shluger, and A. M. Stoneham, J. Phys.: Condens. Matter **5**, 3049 (1993).
[34] G. Pacchioni, F. Frigoli, D. Ricci, and J. A. Weil, Phys. Rev. B **63**, 054102 (2000).
[35] J. Lægsgaard and K. Stokbro, Phys. Rev. Lett. **86**, 2834 (2001).
[36] J. P. Perdew, K. Burke, and M. Ernzerhof, Phys. Rev. Lett. **77**, 3865 (1996).
[37] J. P. Perdew, M. Ernzerhof, and K. Burke, J. Chem. Phys. **105**, 9982 (1996).
[38] P. Broqvist, A. Alkauskas, and A. Pasquarello, Phys. Rev. B **80**, 085114 (2009).
[39] A. Alkauskas, P. Broqvist, F. Devynck, and A. Pasquarello, Phys. Rev. Lett. **101**, 106802 (2008).
[40] A. Alkauskas, P. Broqvist, and A. Pasquarello, Phys. Rev. Lett. **101**, 046405 (2008).
[41] P. Giannozzi, S. Baroni, N. Bonini, M. Calandra, R. Car, C. Cavazzoni, D. Ceresoli, G. L. Chiarotti, I. Dabo, A. Dal Corso, R. Gebauer, C. Gougoussis, A. Kokalj, M. Lazzeri, L. Martin Samos Colomer, N. Marzari, F. Mauri, S. Paolini, A. Pasquarello, L. Paulatto, C. Sbraccia, S. Scandolo, G. Sclauzero, A. P. Seitsonen, A. Smogunov, P. Umari, and R. M. Wentzcovitch, J. Phys. Condens. Matter **21**, 395502 (2009); www.quantum-espresso.org
[42] CPMD version 3.11.1, copyright IBM corp. 1990–2006 and copyright mpi stuttgart (1997–2001).
[43] M. Methfessel and A. T. Paxton, Phys. Rev. B **40**, 3616 (1989).
[44] J. Coutinho, V. J. B. Torres, R. Jones, and P. R. Briddon, Phys. Rev. B **67**, 035205 (2003).
[45] C. G. Van de Walle and J. Neugebauer, J. Appl. Phys. **95**, 3851 (2004).
[46] C. W. M. Castleton, A. Höglund, and S. Mirbt, Phys. Rev. B **73**, 035215 (2006).
[47] S. Lany and A. Zunger, Phys. Rev. B **78**, 235104 (2008).
[48] G. Makov and M. C. Payne, Phys. Rev. B **51**, 4014 (1995).
[49] D. Segev and S.-H. Wei, Phys. Rev. Lett. **91**, 126406 (2003).
[50] T. R. Paudel and W. R. L. Lambrecht, Phys. Rev. B **77**, 205202 (2008).
[51] We define the spin density ρ_{sp} as the difference between the charge densities associated with the two spin polarizations α and β, i.e., $\rho_{sp}=\rho_\beta-\rho_\alpha$.
[52] A. Kokalj, Comput. Mater. Sci. **28**, 155 (2003).
[53] G. Henkelman, B. P. Uberuaga, and H. Jónsson, J. Chem. Phys. **113**, 9901 (2000).
[54] F. Oba, S. R. Nishitani, S. Isotani, H. Adachi, and I. Tanaka, J. Appl. Phys. **90**, 824 (2001).
[55] H. Raebiger, S. Lany, and A. Zunger, Phys. Rev. B **76**, 045209 (2007).
[56] L. S. Vlasenko and G. D. Watkins, Phys. Rev. B **72**, 035203 (2005).
[57] The NEB calculations were performed in supercells of 128 atoms.
[58] G.-Y. Huang, C.-Y. Wang, and J.-T. Wang, Solid State Commun. **149**, 199 (2009).
[59] S. B. Zhang, S.-H. Wei, and A. Zunger, J. Appl. Phys. **83**, 3192 (1998).